Supporting Information:

Two-step assembly kinetics of gold nanoparticles

Jieli Lyu,[†] Damien Alloyeau,[‡] Cyrille Hamon,[*,†] and Doru Constantin[*,†]

†*Université Paris-Saclay, CNRS, Laboratoire de Physique des Solides, 91405 Orsay, France*

‡*Laboratoire Matériaux et Phénomènes Quantiques, Université de Paris - CNRS, F-75013, Paris, France*

E-mail: cyrille.hamon@universite-paris-saclay.fr; doru.constantin@universite-paris-saclay.fr

Particle sizes

We have characterized the particle sizes via absorbance spectroscopy (AS) and transmission electron microscopy (TEM) for the three shapes employed: rods, bipyramids and spheres. We extracted the aspect ratio and its polydispersity from the AS spectra, as shown in Figure S1.

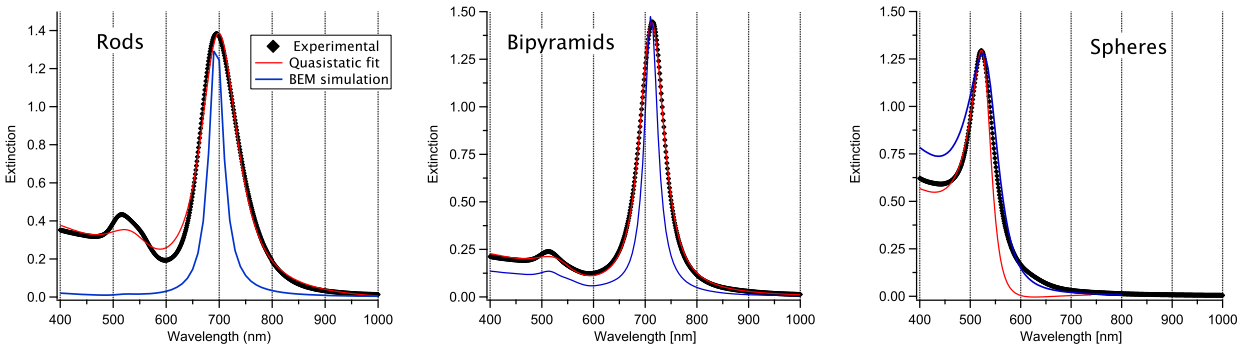

Figure S1: AS spectra for the three particle shapes (from left to right, rods, bipyramids and spheres). Experimental data (diamonds), fits with a quasistatic analytical model (red lines) and BEM simulations (blue lines.)

From the TEM images we extracted the particle diameter (and length for the rods and bipyramids). The corresponding histograms are shown in Figure S2.

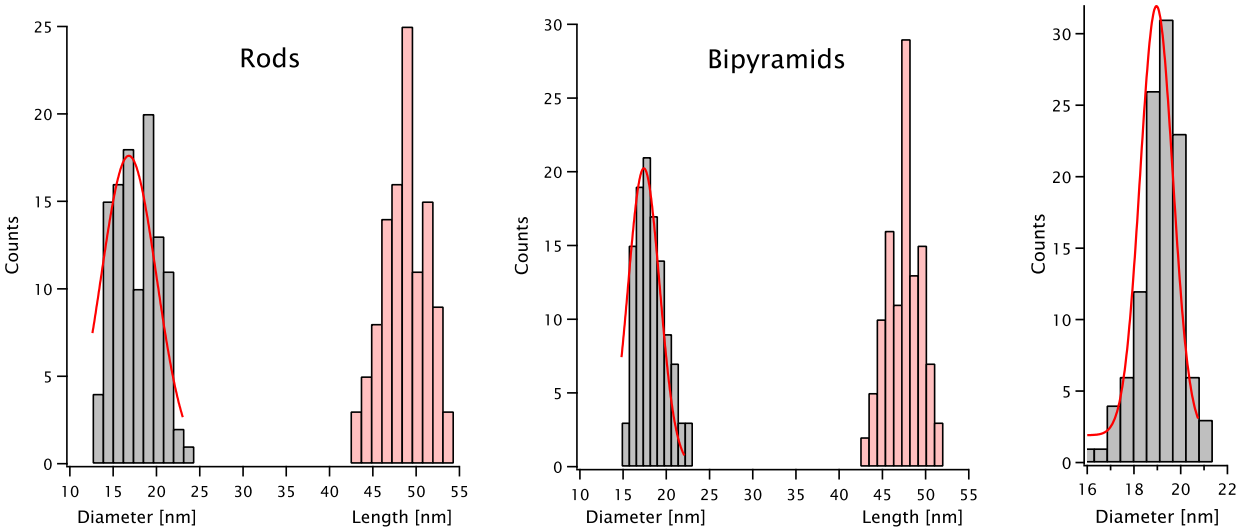

Figure S2: TEM histograms for the three particle shapes (from left to right, rods, bipyramids and spheres). Number of counts for the diameter and length shown as gray and red bars, respectively. Gaussian fits of the diameter distribution (red lines) yield the values given in the main text.

The two methods yield close, but not exactly equal values, as summarized in the main text.

Singular value decomposition

The experimental absorbance data $A(\lambda, t)$ measured as a function of the wavelength λ and the time t can be organized as an $M \times N$ matrix A (we assume in the following that $M > N$), with M wavelength values and N time points, such that A_{ij} is the value for λ_i at t_j, where $t_1 = 0$ and $t_N = t_{\text{final}}$ (the beginning and the end of the kinetics, respectively). Using the singular value decomposition (SVD) technique,[S1] this matrix can be factorized into:

$$\mathsf{A} = \mathsf{U}\,\mathsf{W}\,\mathsf{V}^T\,, \tag{1}$$

where U and V are $M \times M$ and $N \times N$ orthogonal matrices, while W is an $M \times N$ diagonal matrix with non-negative elements $\mathsf{W}_{ii} \geq 0$, known as singular values. The columns of U can be seen as basis vectors that, when multiplied by the time-dependent coefficients in V and weighted by the singular values, yield back the experimental absorbance spectra.

By row and column permutations, we can arrange the singular values such that $\mathsf{W}_{ii} \geq \mathsf{W}_{jj}$ for $i > j$. One can often obtain a very good approximation to A by truncating W to keep only the K largest singular values:

$$\mathsf{A} \simeq \mathsf{A}_K = \mathsf{U}\,\mathsf{W}_K\,\mathsf{V}^T\,, \tag{2}$$

where W_K is obtained from W by setting $\mathsf{W}_{ii} = 0$ for $i > K$. Such a simplification hints that only K species contribute to the absorbance over the duration of the process. The signal of each species, $\mathbf{S}_i(\lambda)$, $i = 1, 2, \ldots, K$ can then be accurately described as a linear combination of the first K columns of U (which form U_K), but the combination coefficients are *a priori* unknown and must be constrained by physical considerations. Explicitly, the signal matrix S given by $\mathsf{S}_{ij} = \mathbf{S}_i(\lambda_j)$ is related to the truncated A_K via a generalized "rotation" matrix R (that includes scale factors): $\mathsf{S} = \mathsf{U}\,\mathsf{W}_K\,\mathsf{R}$ and we can rewrite (2) by inserting the identity

$1 = \mathsf{R}\,\mathsf{R}^{-1}$:

$$\mathsf{A}_K = \mathsf{U}_K\,\mathsf{W}_K\,\mathsf{R}\,\underbrace{\mathsf{R}^{-1}\,\mathsf{V}_K^T}_{\mathsf{C}^T} = \mathsf{S}\,\mathsf{C}^T \tag{3}$$

with C^T the time coefficient matrix. A_K is of size $M \times N$, U_K and S are $M \times K$, W_K, R and R^{-1} are $K \times K$ while V_K^T and C^T are $K \times N$. More intuitively, (3) amounts to writing the experimental absorbance as the sum of K spectra $\mathbf{S}_i(\lambda)$ with the time-varying coefficients $\mathbf{C}_i(t)$.

$$\mathsf{A}(\lambda_m, t_n) = \sum_{i=1}^{K} \mathbf{C}_i(t_n)\mathbf{S}_i(\lambda_m) \tag{4}$$

The first condition we impose on matrix R is that one of the basis spectra (say, $\mathbf{S}_1$) is simply the first column of U_K (since only the first species is present in the beginning; we assume here that the time before sample preparation and first acquisition is much shorter than the typical reaction time.) More precisely,

$$\mathsf{C}^T{}_{i1} = [\mathsf{R}^{-1}\,\mathsf{V}_K^T]_{i1} = (1, 0, 0, \ldots, 0)^T \tag{5}$$

fixing K elements of R.

A second condition is due to the total amount of gold being constant. It is known that the extinction of gold nanoparticle solutions at a wavelength $\lambda_{\text{norm}} \simeq 450\,\text{nm}$ is relatively independent of the shape, size and aggregation state of the objects,[S2] thus providing a robust way of quantifying their concentration. We therefore normalize the second and subsequent components such that $\mathbf{S}_i(\lambda_{\text{norm}}) = \mathbf{S}_1(\lambda_{\text{norm}})$. This fixes another $K - 1$ elements of R.

In this work, we choose $K = 2$, which yields good results and is easily interpreted in terms of the conversion between an initial population (consisting of isolated particles) and a final one of aggregates. The final relation stems is that $\mathbf{S}_2$ be free of any contribution from $\mathbf{S}_1$: we adjust R (by hand) so that $\mathbf{S}_2$ has no peak at the position of the LSPR of the isolated particles for rods and bipyramids. This last condition completely defines R.

The situation is more complicated for spheres, because the isolated objects have three

equivalent space directions, so their spectrum is $\mathbf{S}_1 = \frac{1}{3}\,3\mathbf{S}_{\rm iso}$, while those assembled into chains are described by $\mathbf{S}_2 = \frac{1}{3}\,(2\mathbf{S}_{\rm iso} + \mathbf{S}_{\rm coupl})$ where $\mathbf{S}_{\rm coupl}$ is the (red-shifted) coupled plasmon resonance excited when the incident polarization is along the chain.

Applying here the final relation used for rods and bipyramids yields a spectrum matrix S containing the two distinct **modes** $\mathbf{S}_{\rm iso}$ and $\mathbf{S}_{\rm coupl}$. Since we are interested in the two **populations** (isolated and chained objects), we must "remix" the modes in the proportions defined above, by inserting into Eq. (3) the matrix $\mathsf{M} = \begin{pmatrix} 1 & 2/3 \\ 0 & 1/3 \end{pmatrix}$ to yield:

$$\mathsf{A}_K = \mathsf{S}\,\mathsf{M}\,\mathsf{M}^{-1}\,\mathsf{C}^T = \mathsf{S}'\,\mathsf{C}'^T \tag{6}$$

The resulting S' now contains the desired $\mathbf{S}'_1$ and $\mathbf{S}'_2$, while C'^T holds the corresponding time coefficients.

Modeling the AS data: goodness-of-fit and reaction order

We determined the reaction order by fitting the time coefficient of the isolated particle concentration $C_1(t)$ with an exponential $\eta \exp(-kt) + (1 - \eta)$ and a reciprocal function $\frac{\eta}{1 + t/t_{1/2}} + (1 - \eta)$ (corresponding to first-order and second-order kinetics, respectively.) Each function has two free parameters: the yield η (constrained to the $[0, 1]$ interval), the rate constant k for the first-order kinetics and the half-time $t_{1/2}$ for the second-order kinetics. The fits are shown in Figure S3 for various c_{Au} values and the corresponding goodness-of-fit parameter χ^2 is displayed in Figure S4. Below $c_{\mathrm{Au}} = 0.15\,\mathrm{mM}$, the exponential model is clearly better than the reciprocal one, while above 0.25 mM the quality fit is indistinguishable. We conclude that the data is better described by first-order kinetics.

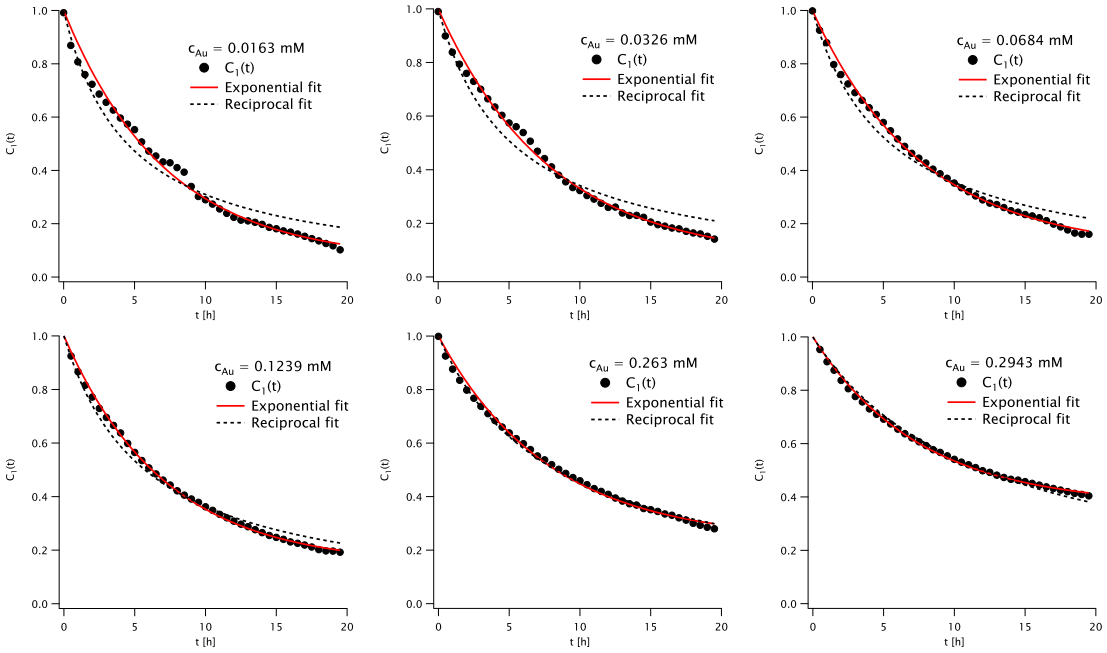

Figure S3: Fit of the time coefficient of the isolated particle concentration $C_1(t)$ (dots) with an exponential (solid red line) and a reciprocal (black dashed line) function. The c_{Au} values are indicated in each panel.

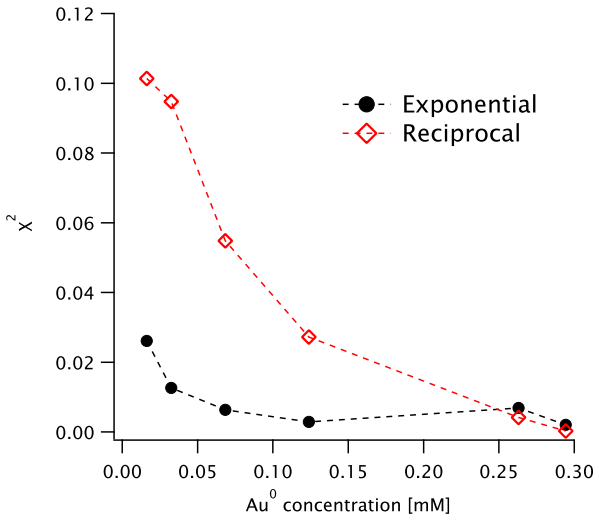

Figure S4: Goodness-of-fit values χ^2 corresponding to the fits in Figure S3.

Plasmon coupling simulations

In the main text, we attribute the changes in AS spectra of the particles to coupling of the plasmon modes. This coupling is extremely sensitive to the reciprocal position and orientation of the objects, as shown below. All simulations are performed using the MNPBEM toolbox.[S3] The dielectric constant for gold is that given by Johnson and Christy[S4] (with no finite-size correction) and the host medium is water. In Figures S6a) and S7 we report the extinction efficiency Q_{ext}, defined as the ratio of the extinction cross-section C_{ext} to the geometrical cross-section of the particle.

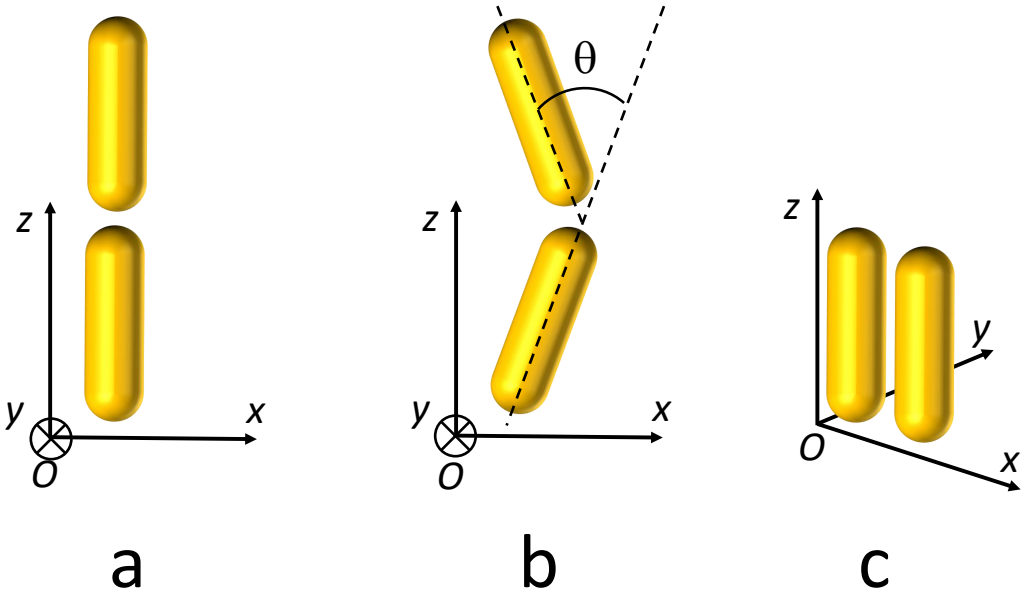

Figure S5: System geometry for the plasmon coupling simulations, in a) tip-to-tip b) tilted and c) side-to-side configuration of a particle dimer.

Tip-to-tip assembly

It is well-known that tip-to-tip assembly of nanorods leads to a red shift of their longitudinal plasmon resonance.[S5] In this section we quantify the shift as a function of separation distance and number of particles in the chain for the nanorod morphology used in our experiments

(see the main text.) We also discuss briefly the effect of misalignment (axis tilt.)

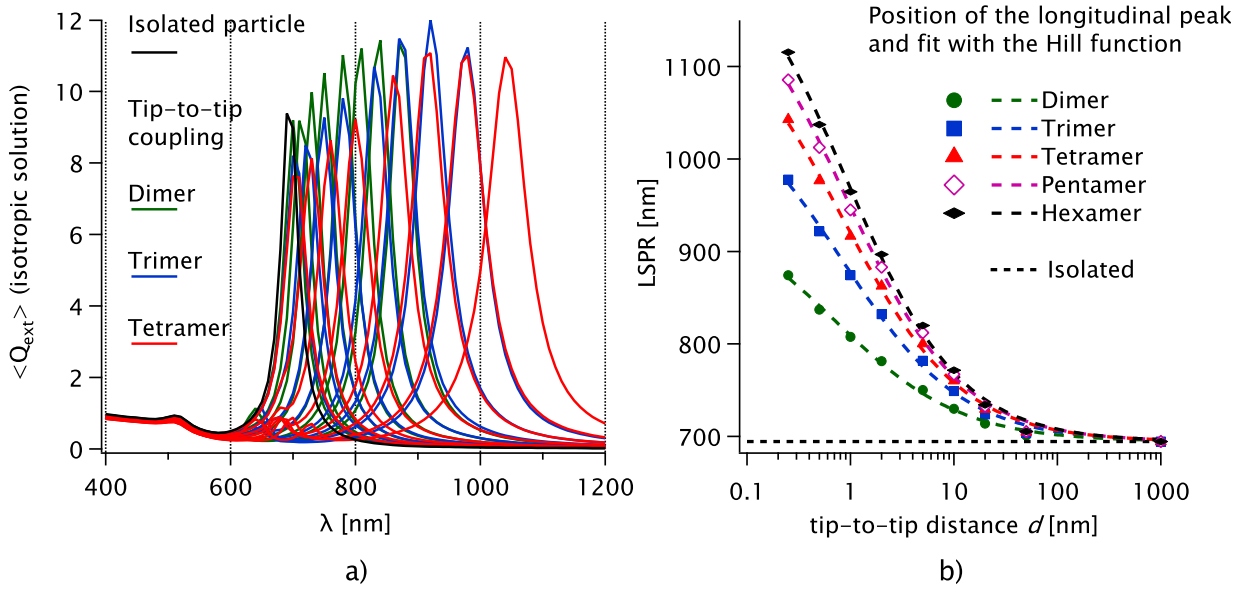

Figure S6: a) Simulated extinction spectra for an isolated gold spherocylinder with aspect ratio $AR = L/D = 2.9$ (black line) and for a tip-to-tip dimer, trimer and tetramer of such objects with a minimal surface separation d varying from 50 to 0.25 nm (green, blue and red line, respectively). b) Position of the longitudinal peak (LSPR) as a function of the surface separation d for dimer to hexamer (symbols) and fits with the Hill equation.

Empirically, we find that the dependence of the peak maximum on the interparticle separation $\lambda_{\max}(d)$ is much better described by the Hill equation:[S6]

$$\lambda_{\max}(d) = \lambda_{\max}(\infty) + \frac{\lambda_{\max}(0) - \lambda_{\max}(\infty)}{1 + \left(\frac{d}{d_{\text{half}}}\right)^{\alpha}} \tag{7}$$

rather than, say, a decaying exponential, with $d_{\text{half}} \simeq 0.7 - 0.9\,\text{nm}$ and $\alpha \simeq 0.7$. $\lambda_{\max}(0)$ is about 950 nm for the dimer, 1100 nm for the trimer and 1260 nm for the hexamer. The baseline value $\lambda_{\max}(\infty) = 694.37\,\text{nm}$ is constrained at the peak position for an isolated object. For comparison, the peak position for solid rods (welded oligomers) of the same length are $\lambda_{\max} = 1018$, 1289 and 1530 nm for the dimer, trimer and tetramer, respectively.

It is worth comparing our results to those of Abtahi et al., Ref S7: they model nanorod oligomers (consisting of k particles of length L) as solid gold rods of length kL and obtain

coupled longitudinal peaks in the 850-1050 nm range for dimers, trimers and tetramers (for rods with an initial aspect ratio $AR = 4.4$.) This is surprising, because for a rod with $AR = 8.8$ (their model for a dimer), the longitudinal peak is above 1200 nm,[S8] and not at 860 nm, as indicated in their Fig. S5.

We believe the error lies in the calculation of the extinction γ'' on page 8 of the SI for Ref. S7: if the dielectric constant of the medium ϵ_m is taken as 1 (for air) then the expression $(1 - P_j)/P_j\,\epsilon_m \simeq 40$, requiring $\epsilon_1 = -40$ (achieved at about 860 nm, close to the authors' result). However, water has $\epsilon_m = 1.77$, so that $(1 - P_j)/P_j\,\epsilon_m \simeq 70$, and the resonance condition $\epsilon_1 = -70$ is achieved at about 1240 nm. It looks like the spectra for the dimer, trimer etc. were calculated in air, while the monomer has the correct value for water environment.

Side-to-side assembly

When the particles are in a side-to-side configuration, the longitudinal plasmon resonance is blue-shifted and a very small (note the logarithmic scale) red-shifted peak appears, as shown in Figure S7 for an interparticle distance of 2 nm.

Tilt effect

Aside from the tip-to-tip and side-to-side configurations, the particles can of course be tilted, with an angle θ between 0 and π (see Figure S5b.) We simulated a dimer with a constant minimal surface separation $d = 2\,\mathrm{nm}$, for different tilt angles θ (Figure S8.) As already shown in the literature,[S9] the spectra have two well-defined peaks, corresponding to the bonding and anti-bonding plasmon modes (observed in the tip-to-tip and side-to-side configurations, respectively) with varying amplitudes. Thus, particle tilt changes the relative amplitude of these modes in the final spectrum but not their position so it is not relevant for our discussion in the main text.

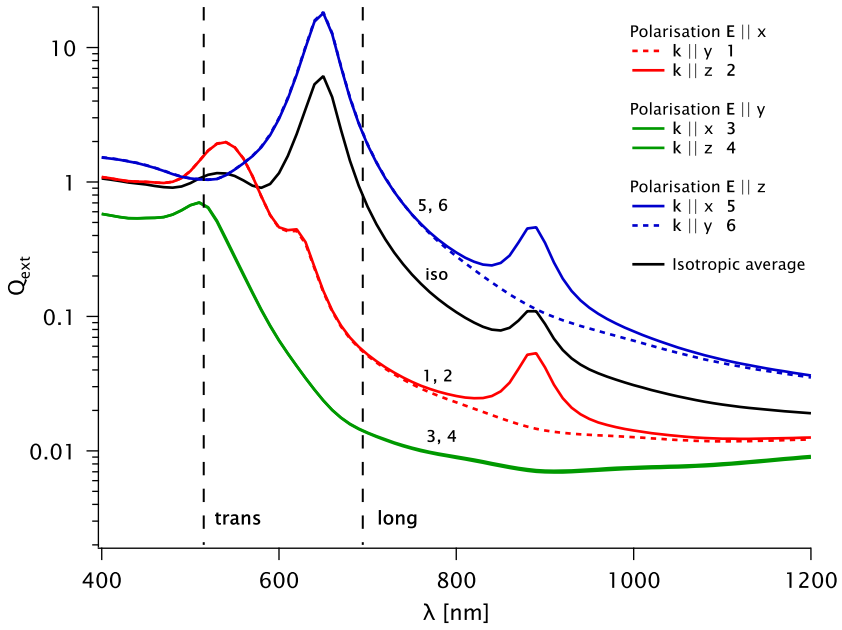

Figure S7: Simulated extinction spectra for a side-to-side dimer, with a minimal surface separation $d = 2\,\text{nm}$, for different directions and polarizations of the incident beam (different colors); see Figure S5 for the geometry. The isotropic average is shown as solid black line. The positions of the transverse and longitudinal peaks for the isolated particle are shown as dashed lines.

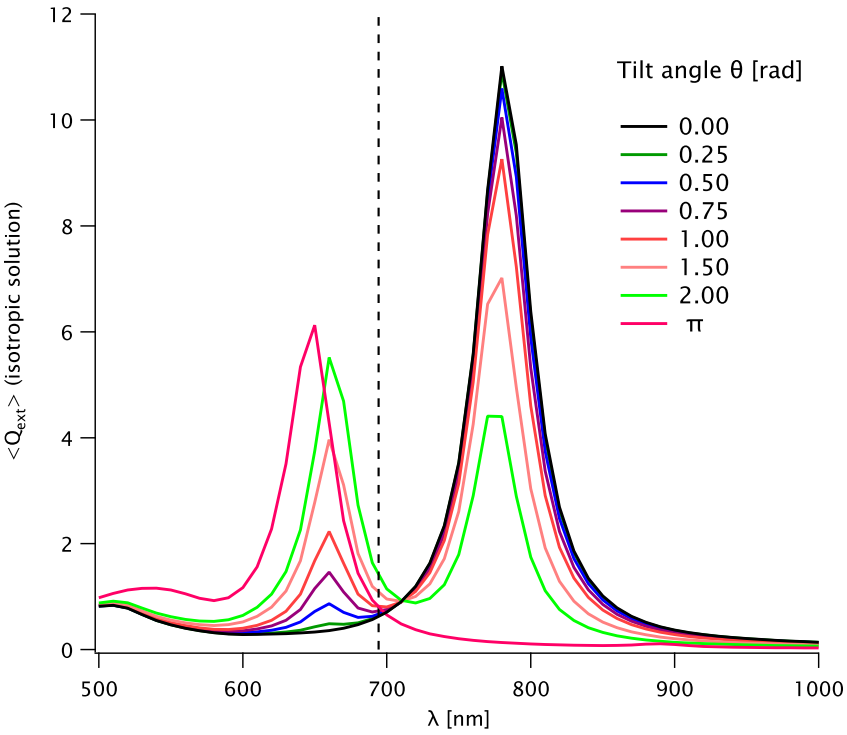

Figure S8: Simulated extinction spectra for a dimer, with a minimal surface separation $d = 2\,\mathrm{nm}$, for different tilt angles θ indicated on the graph (different colors); see Figure S5 for the geometry. The position of the longitudinal peak for the isolated particle is shown as dashed line.

Sphere coupling

For sphere assemblies we performed an analysis similar to that done for rods in the main text, but for clarity we consider the spectra $\mathbf{S}_2(\lambda)$ of the coupled modes, before applying the "mixing matrix" M as discussed above to yield the physical spectra $\mathbf{S'}_2(\lambda)$ of the chains. This data is shown in Figure S9 and, as for rods, exhibits two bands (shaded in gray) red-shifted with respect to the peak of the isolated particles (dashed line) by about 35 and 130 nm. There may be a slightly blue-shifted band (by less than 10 nm), but its amplitude is very low.

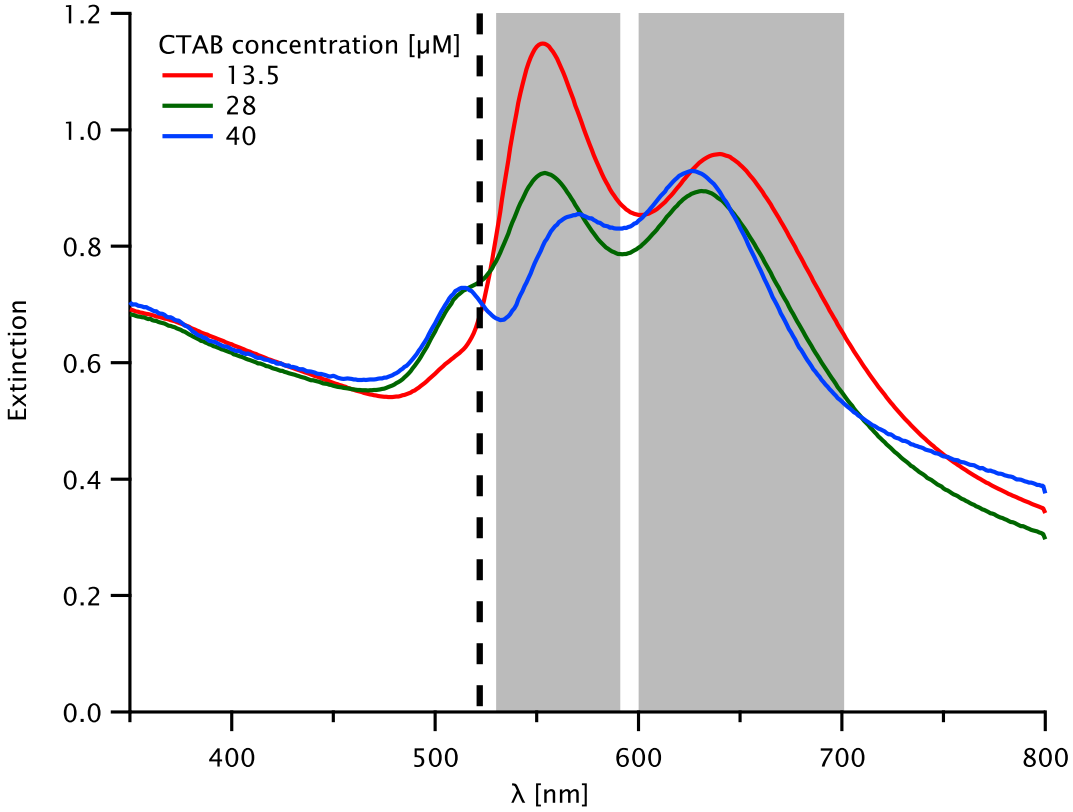

Figure S9: Extinction spectra $\mathbf{S}_2(\lambda)$ of the coupled modes of sphere assemblies, for various CTAB concentrations (different colors). The position of the plasmon peak for the isolated particle is shown as dashed line. Relevant plasmon bands are marked by gray shading (see text.)

Based on MNPBEM simulations of sphere chains with varying particle number and spacing (Figure S10) we conclude that the red-shifted bands correspond to an interparticle dis-

tance d of above 2 nm (consistent with one bilayer thickness) and below 0.5 nm (less than one monolayer), with the same interpretation as for nanorods.

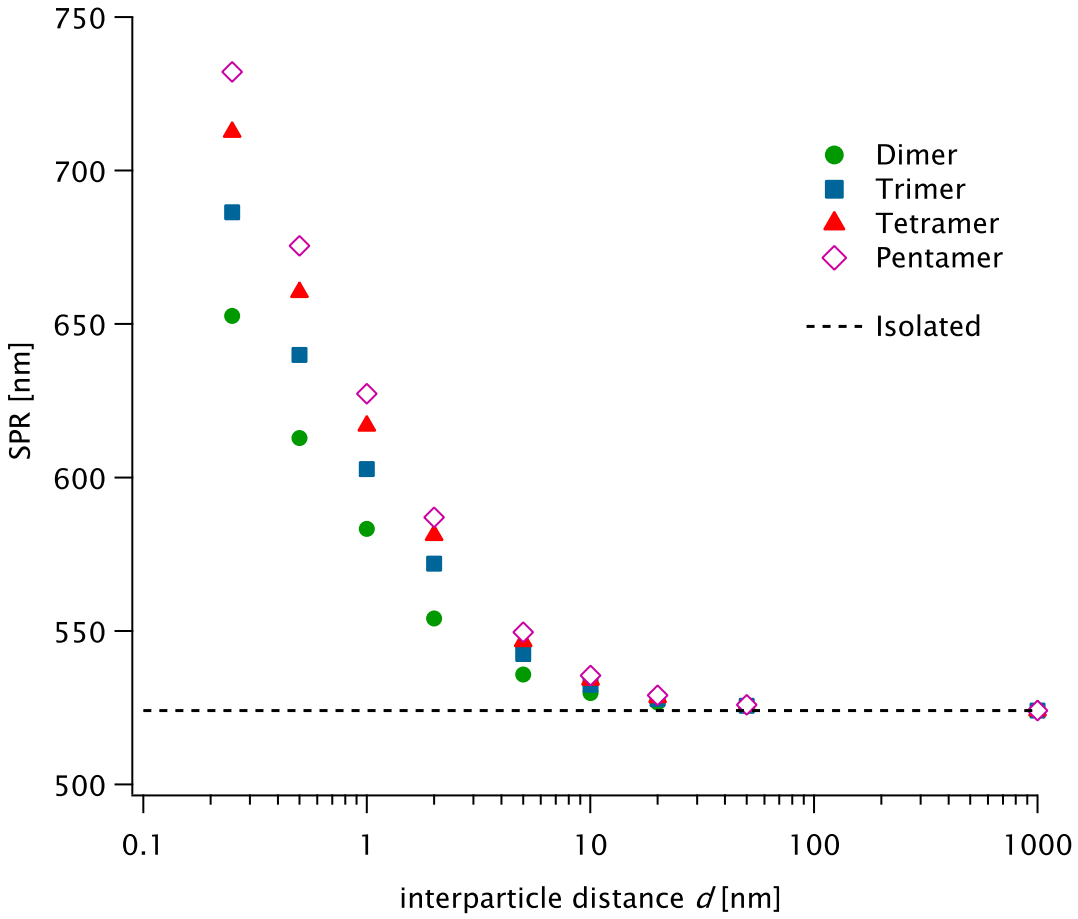

Figure S10: Position of the coupled peak as a function of the surface separation d between spheres for dimer to pentamer chains (symbols)

Dialysis tests

We assembled GNR chains at $c_{\mathrm{Au}} = 0.125\,\mathrm{mM}$ in 14.3 μM CTAB with 1 mM $MgSO_4$. After 20h, we stopped the assembly process by adding CTAC to a final 10 mM concentration. We then inserted 2 mL of chain solution in a dialysis bag (MWCO 10K, flat width: 32 mm, Spectrum Laboratories, Inc., CA, USA), sealed the ends with clips and placed it in 1 L of an aqueous solution with the same surfactant concentration (10 mM CTAC and 14.3 μM CTAB). We also prepared a reference sample in the same conditions but without $MgSO_4$. We renewed the dialysis solution twice a day. After 1 week, we retrieved the chain solution and reference sample from their dialysis bags. AS spectra were measured immediately after preparation (0h), after 20h and after dialysis.

From the UV/vis spectrum, the intensity of LSPR of chains solution changed from 0.72 to 0.41, and the intensity of LSPR of reference sample changed from 1.42 to 0.91. The decrease in intensity is due to the change in the concentration of the solution in the dialysis bag under the effect of osmotic pressure.

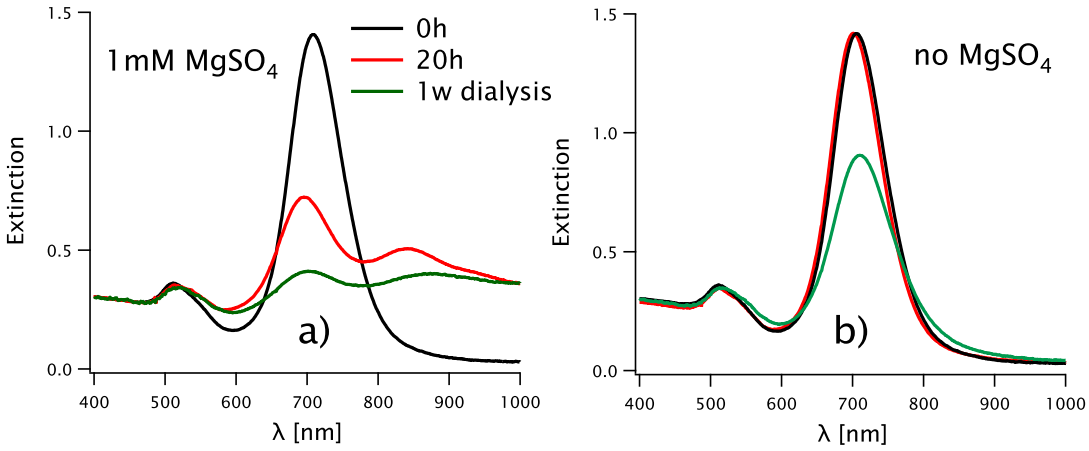

Figure S11: AS results for dialyzed samples: a) with 1 mM $MgSO_4$ and b) without $MgSO_4$. In both panels we show the initial spectrum (black), the one after 20h of reaction (red) and the one after a subsequent 1w dialysis (green).

Analysis of the LCTEM videos

We measured the tip to tip and side to side distances between bipyramids in water by LCTEM. Most of the time, the tip to tip distances were undetectable (Figure S12a). In our high frame rate imaging conditions, the resolution obtained on gold nanoparticles is around 1 nm, suggesting that the tip to tip distance is below this value. Occasionally, we could detect tip to tip distances between 1 and 2 nm (Figure S12b). The side to side distances can always be measured and vary between 2 and 5 nm (Figure S12c and S S12d).

We show in Figure S13 the raw data extracted from the LCTEM movie of the dimer in Figure 9a of the main text and the associated histograms for the center-to-center distance and the angle between the bipyramid long axis and the line through the centers of the two particles. The Gaussian fit of the histograms yields the values in Figure 9c and d.

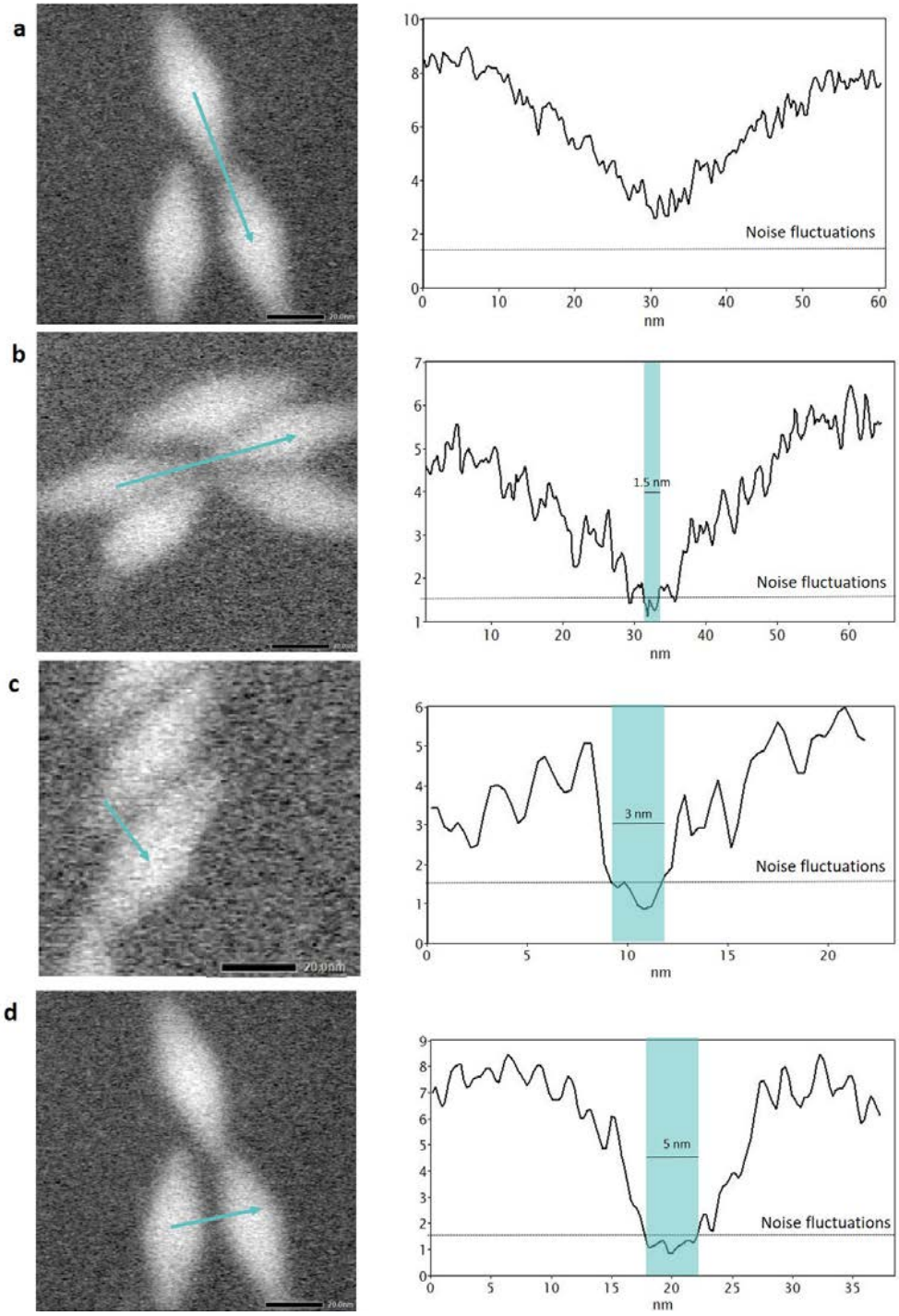

Figure S12: Measurements of tip to tip (a, b) and side to side (c, d) distances between gold bipyramids in water. (Left) LCTEM images of particle chains extracted from videos acquired with a frame rate of 25 images per second. (Right) Signal-to-noise ratio profiles measured along the arrows shown on the images. The gap between the nanoparticles is indicated in blue on the profile. It corresponds to the area where the signal to noise ratio goes below the noise fluctuations measured in the image areas where there are no nanoparticles (< 1.5).

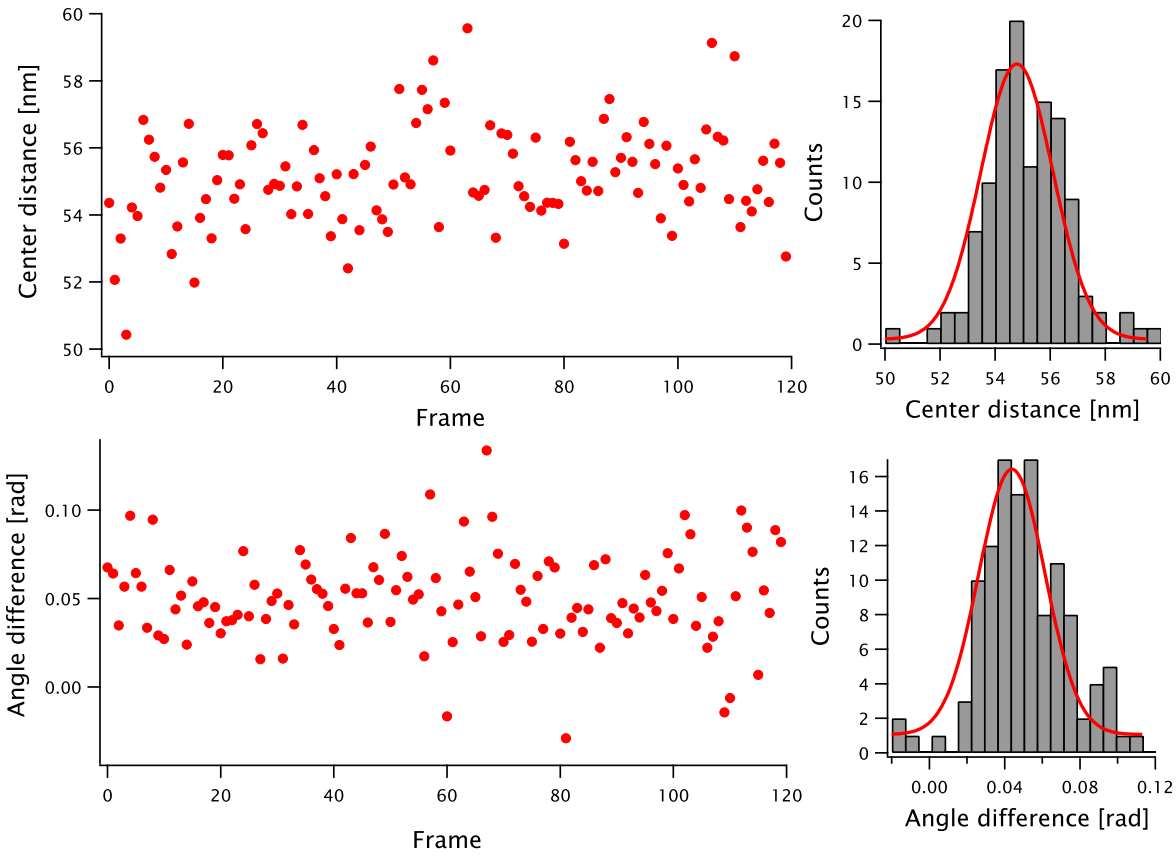

Figure S13: Left: raw data for the bipyramid-sphere dimer in Figure 9a of the main text: Center-to-center distance (top) and angle between the bipyramid long axis and the line through the centers of the two particles (bottom). Right: Histograms of the two parameters (bars) and Gaussian fits (red lines.)

References

(S1) Press, W. H. *Numerical recipes in C: the art of scientific computing*; Cambridge University Press: Cambridge; New York, 1992.

(S2) Haiss, W.; Thanh, N. T. K.; Aveyard, J.; Fernig, D. G. Determination of Size and Concentration of Gold Nanoparticles from UV-Vis Spectra. *Analytical Chemistry* **2007**, *79*, 4215–4221.

(S3) Hohenester, U.; Trügler, A. MNPBEM–A Matlab toolbox for the simulation of plasmonic nanoparticles. *Computer Physics Communications* **2012**, *183*, 370–381.

(S4) Johnson, P. B.; Christy, R. W. Optical Constants of the Noble Metals. *Physical Review B* **1972**, *6*, 4370–4379.

(S5) Liu, K.; Ahmed, A.; Chung, S.; Sugikawa, K.; Wu, G.; Nie, Z.; Gordon, R.; Kumacheva, E. *In Situ* Plasmonic Counter for Polymerization of Chains of Gold Nanorods in Solution. *ACS Nano* **2013**, *7*, 5901–5910.

(S6) Gesztelyi, R.; Zsuga, J.; Kemeny-Beke, A.; Varga, B.; Juhasz, B.; Tosaki, A. The Hill Equation and the Origin of Quantitative Pharmacology. *Archive for History of Exact Sciences* **2012**, *66*, 427–438.

(S7) Abtahi, S. M. H.; Burrows, N. D.; Idesis, F. A.; Murphy, C. J.; Saleh, N. B.; Vikesland, P. J. Sulfate Mediated End-to-End Assembly of Gold Nanorods. *Langmuir* **2017**,

(S8) Constantin, D. Why the Aspect Ratio? Shape Equivalence for the Extinction Spectra of Gold Nanoparticles. *The European Physical Journal E* **2015**, *38*, 116.

(S9) Shao, L.; Woo, K. C.; Chen, H.; Jin, Z.; Wang, J.; Lin, H.-Q. Angle- and Energy-Resolved Plasmon Coupling in Gold Nanorod Dimers. *ACS Nano* **2010**, *4*, 3053–3062.